Journal of Alloys and Compounds 726 (2017) 1147–1154

Contents lists available at ScienceDirect

Journal of Alloys and Compounds

journal homepage: http://www.elsevier.com/locate/jalcom

Au-$BiOCl_{1-x}Br_x$ composites with highly enhanced photocatalytic activity for phenol decomposition

Yi Ling Qi [a], Yi Fan Zheng [b], Xu Chun Song [a, *]

[a] Department of Chemistry, Fujian Normal University, Fuzhou 350007, PR China
[b] Research Center of Analysis and Measurement, Zhejiang University of Technology, Hangzhou 310014, PR China

ARTICLE INFO

Article history:
Received 30 April 2017
Received in revised form
24 July 2017
Accepted 10 August 2017
Available online 12 August 2017

Keywords:
Au NPs
$BiOCl_{1-x}Br_x$
SPR effect
Photocatalytic

ABSTRACT

Au nanoparticles (Au NPs) were deposited onto $BiOCl_{1-x}Br_x$ nanosheets by using a facile ultrasonic treatment. The obtained Au-$BiOCl_{1-x}Br_x$ composites exhibit excellent photocatalytic property in the reaction of decomposing phenol aqueous solution under simulated solar light irradiation. There is a positive relationship exists in the surface plasmon resonance (SPR) of Au NPs and enhanced activities, which is contributed to the separation of photo-induced electrons and holes as well as facilitate the absorption of visible light. In addition, the tunable energy band structure might be beneficial to enhance the photocatalytic activities of Au-$BiOCl_{1-x}Br_x$ composites for optimizing the bandgap. And the •OH and h^+ species were the main active species in photocatalytic reactions. In this paper, the Au-$BiOCl_{1-x}Br_x$ photocatalysts were demonstrated to be a promising material for practical applications in the purification of organic pollutants.

1. Introduction

As we know, the shortage and pollution of water resources become a serious problem for human health. Phenol and phenolic compounds as one of organic pollutants can accumulate over several decades in the presence of the wastewater [1–3]. In recent decades, heterogeneous photocatalysis has been regarded as a green and promising chemical process for degration of organic contaminants. Among various photocatalytic materials, as novel ternary oxide semiconductors, BiOX (X = Cl, Br and I) have evoked much interests for the potential photocatalytic abilities [4–6]. Bismuth oxyhalides are characterized by a layered structure where halogen atoms are existed between $[Bi_2O_2]^{2+}$ layers [7–10]. And the structure is believed to favor the efficient separation of photo-induced electron-hole pairs due to the formation of internal electric fields, thus improving the photocatalytic activity [11–13]. However, the photoelectrochemical properties of individually BiOX are not still satisfactory for practical applications. In order to conquer the shortcoming, some strategies have been employed to improve the photoelectrochemical properties, such as controlled synthesis of BiOX with specific morphology, doping of noble metal, semiconductor recombination and so on. In addition, the BiO-Cl_xBr_{1-x} [14], $BiOCl_xI_{1-x}$ [15] and $BiOBr_xI_{1-x}$ [16] solid solutions have been synthesized recently, and all the solid solutions have been believed to be more active than the pure forms. The possible reasons for the high photocatalytic performance of these solid solutions are found to have suitable energy band edge. Nevertheless, the researches concerning $BiOCl_xBr_{1-x}$ are still scarce up to now, and the light absorption of UV-activated semiconductors (e.g. BiOCl) still exists in the solid solutions. Therefore, it is still obligatory to further enhance their photocatalytic activity for practical applications.

Noble metal-modified semiconductor materials have drawn a large quantity of attention for optimizing the photocatalytic reactions recently. In particular, nanoparticles of noble metals can exhibit a surface plasmon resonance (SPR), which increases optical absorption [17]. Among modified noble metals, gold (Au) is one of the most suitable metals in terms of its electrical conductivity, good biocompatibility and chemical activity. The interaction between the noble metal gold nanoparticles (Au NPs) and semiconductors has been considered to have high Schottky barriers [18], and Au NPs act as an electron sink which promotes the separation of photoinduced electron-hole pairs and facilitates interfacial electron transfer. Considering the significant advantage of Au NPs and to realize a compact metal/semiconductor interface, some synthetic strategies were taken to load the metals on semiconductors surface.

* Corresponding author.
E-mail address: songxuchunfj@163.com (X.C. Song).

http://dx.doi.org/10.1016/j.jallcom.2017.08.081
0925-8388/

Construction of metal-modified semiconductor via photoreduction method has been proved a useful way, such as Au/BiOCl [19–21], Au/CdS [22], Au/TiO_2 [23], Au/ZnO [24,25] and Au/$BiOBr_{0.2}I_{0.8}$ [18] have turned out to broaden the visible light absorption and enhance the photocatalytic activity. However, no report has been made the photocatalytic performance about the decoration of Au on the $BiOCl_{1-x}Br_x$ solid solutions as far as we know.

Herein, we use a facile method to prepare Au-$BiOCl_{1-x}Br_x$ composites by precipitation and assisted sonication methods. All Au-loaded catalysts have significant light absorbance in visible light region, and show significant improvement of photocatalytic activity for degrading phenol solution under simulated solar light irradiation. And the photodegradation efficiency of the obtained Au-$BiOCl_{0.25}Br_{0.75}$ composites can achieve 98.5% after 75min of simulated solar light irradiation. The possible mechanism of photocatalytic property enhancement and the SPR effect of Au deposition were further investigated.

2. Experimental section

2.1. Synthesis of $BiOCl_{1-x}Br_x$ solid solutions

The $BiOCl_{1-x}Br_x$ (x = 0, 0.25, 0.5, 0.75, 1) with a sheet structure were synthesized by using a precipitation method at 85 °C. Firstly, 10 mmol of $Bi(NO_3)_3 \cdot 5H_2O$ (4.8508 g) was added to 20 mL ethylene glycol (EG) with constant stirring. Then stoichiometric amounts of potassium chloride (KCl) and potassium bromide (KBr) were added to 20 mL distilled water. Subsequently, the latter aqueous was added into the former solution. Finally, place the mixtures in 85 °C water bath with continuous stirring for 5 h. After that, the precipitations were separated by centrifugation when cooling to room temperature naturally. Wash the products with distilled water and absolute alcohol three times and dried at 80 °C overnight. The BiOCl, $BiOCl_{0.25}Br_{0.75}$, $BiOCl_{0.5}Br_{0.5}$, $BiOCl_{0.75}Br_{0.25}$ and BiOBr were successfully collected.

2.2. Synthesis of $BiOCl_{1-x}Br_x$ decorated with Au nanoparticles

Au nanoparticles were prepared by following steps: Firstly, 0.04 g gold chloride hydrate powder ($AuCl_3$) was added to 200 mL distilled water with strongly stirring. The temperature gradually rose to the boiling point of $AuCl_3$ solution and it remained to boil for 30 min. Then, 0.3423 g trisodium citric dehydrate ($C_6H_5Na_3O_7$) was dissolved in 30 mL of deionized water and added into the above solution. And the solution was continued to boiling until the color varied from transparent to palered, which indicating the formation of Au NPs. To prepare Au-$BiOCl_{1-x}Br_x$, 0.3 g $BiOCl_{1-x}Br_x$ (x = 0, 0.25, 0.5, 0.75, 1) samples were added to the Au NPs solution (15, 30, 45 mL), respectively. The Au/$BiOCl_{1-x}Br_x$ samples with different weight ratios were estimated to be 0.65, 1.3, 1.95%, respectively. Then the suspension was sonicated for 1 h to promote the dispersion and to load the Au NPs on the $BiOCl_{1-x}Br_x$ sheets. Finally, the Au-$BiOCl_{1-x}Br_x$ composites were obtained by centrifugation, washed, dried and collected.

2.3. Characterization

Crystal structure identification of the as-synthesized samples was recorded on a Thermo ARL SCINTAG X'TRA with Cu Ka X-ray source (λ = 1.5406 Å) operating at 40 kV and 40 mA. The morphologies of $BiOCl_{1-x}Br_x$ and Au-$BiOCl_{1-x}Br_x$ composites were observed by a Hitachi S-4700 scanning electron microscopy (SEM) and Tecnai G2 F30 high resolution transmission electron microscopy (HRTEM). Energy-dispersive X-ray spectroscopy (EDS,

Fig. 1. XRD patterns of (a) $BiOCl_{1-x}Br_x$ (x = 0, 0.25, 0.5, 0.75 and 1) solid solutions; (b) 1.3% Au-$BiOCl_{1-x}Br_x$ composites (c) the expanded XRD patterns of Au-$BiOCl_{0.25}Br_{0.75}$ in the range of 2θ = 35–47°.

Thermo Noran VANTAG-ESI) data were obtained to investigate elemental composition. The ultraviolet visible diffuse reflectance spectrums were measured on a Lambda 850 UV–vis spectrophotometer in the range of 200–800 nm, $BaSO_4$ was used as reference standard material. Photoelectrochemical characterization was characterized on a CHI-650E electrochemical workstation (Shanghai, China) with a standard three-electrode system. The prepared samples acted as the working electrode. The counter electrode and reference electrode were platinum wire and Ag/AgCl electrode, and 0.1 M Na_2SO_4 was used as electrolyte.

2.4. Photocatalytic experiments

The photocatalytic activity of all the composites was estimated by degradation of phenol aqueous solution under simulated solar light irradiation. For all reactions, 0.1 g photocatalyst was added into 50 mL of phenol solution (25 mg/L) in a beaker. Each experiment consisted of powdered catalyst with the phenol solution for 30 min with constantly stirring to obtain the adsorption-desorption equilibrium. Then, the mixed solution was exposed to simulated solar light irradiation while stirring. Subsequently, the suspensions (2–3 mL) were collected into centrifuge tubes at intervals of 15 min during irradiation time for spectrophotometric analysis. Finally, the suspensions were centrifuged and analyzed on the UV759S UV–vis spectrometer.

3. Results and discussion

The X-ray diffraction patterns of the as-synthesized $BiOCl_{1-x}Br_x$ ($x = 0$, 0.25, 0.5, 0.75 and 1) samples and 1.3% Au-$BiOCl_{1-x}Br_x$ photocatalysts are shown in Fig. 1. Typical XRD patterns of BiO-$Cl_{1-x}Br_x$ for $x = 0$ and 1 are well indexed to those reported for BiOCl (JCPDS No. 06-0249) and BiOBr (JCPDS No. 09-0393), respectively. All samples exhibit sharp diffraction peak shapes, indicating high crystallinity as shown in Fig. 1a. With increasing x, the sharp diffraction peaks shift gradually to smaller-angle side, which suggesting the samples are not mixtures of BiOCl and BiOBr phases but $BiOCl_{1-x}Br_x$ solid solutions. The radius of Cl^- (1.81 Å) is smaller than that of Br^- (1.96 Å), so it can be considered that the Cl^- incorporated in BiOBr lattice or entered into its interstitial sites. Fig. 1b displays that the peak intensity and position of the 1.3% Au-$BiOCl_{1-x}Br_x$ photocatalysts do not change much with the deposition of Au. No obvious Au peaks were detected, implying that Au has no significant influence on the crystal structure of $BiOCl_{1-x}Br_x$ solid solutions, which might be ascribed to the low Au content and small size of Au NPs as well as Au NPs distributed uniformly in the surface of $BiOCl_{1-x}Br_x$ solid solutions. As for the existence of Au, it can be further demonstrated the following expanded XRD patterns of Au-$BiOCl_{0.25}Br_{0.75}$ photocatalyst in Fig. 1c, which resulting from the block diagram of Fig. 1b. In the range of $2\theta = 35–47^\circ$, the peak at 2θ of 39.6°, 45.8° and 46.4°are indexed to (112), (200) and (113) planes of $BiOCl_{0.25}Br_{0.75}$, respectively. And the diffraction peak (2θ) at 38.1° can be indexed to that of metallic Au (JCPDS No. 71-4615) and correspond to (111) plane, which indicating the existence of metallic Au in Au-$BiOCl_{1-x}Br_x$ composites.

The morphologies of as-synthesized $BiOCl_{0.25}Br_{0.75}$ and 1.3% Au-$BiOCl_{0.25}Br_{0.75}$ composites have been characterized by SEM analysis. As shown in Fig. 2a, the $BiOCl_{0.25}Br_{0.75}$ has a sheet-like

Fig. 2. SEM images of (a) $BiOCl_{0.25}Br_{0.75}$, (b) 1.3% Au-$BiOCl_{0.25}Br_{0.75}$, respectively; (c) the element mapping of 1.3% Au-$BiOCl_{0.25}Br_{0.75}$; and (d) HRTEM image of 1.3% Au-$BiOCl_{0.25}Br_{0.75}$ composite.

architecture with the diameter of about 100–300 nm. Also, Au deposition process brings no observable transformation to the morphology of the $BiOCl_{0.25}Br_{0.75}$ samples (Fig. 2b). It is obviously observed that Au nanoparticles (Au NPs) are deposited randomly on the surface of the $BiOCl_{0.25}Br_{0.75}$ samples as can be seen in Fig. 2b. The sizes of Au NPs are calculated approximately 50–70 nm. The chemical element mapping analysis is used to further confirm the composition of the composites. As shown in Fig. 2c, it directly represents elemental mapping images of O, Cl, Br, Au and Bi elements, respectively. It can be seen that Au NPs are homogenously distributed on the $BiOCl_{0.25}Br_{0.75}$ nanosheets. The high-resolution TEM (HRTEM) image in Fig. 2d shows the high crystallinity of the

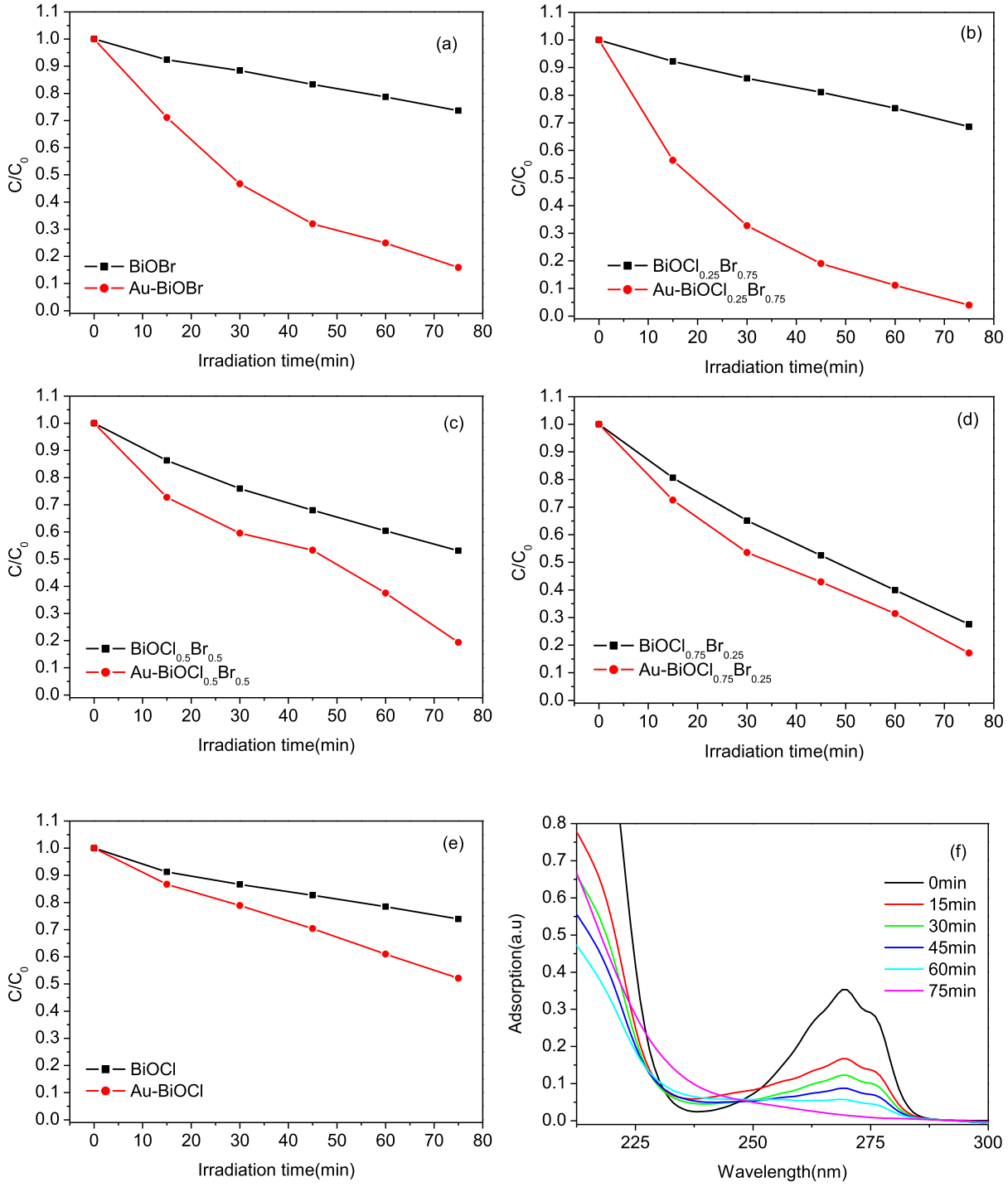

Fig. 3. (a)–(e) The plot of C/C_0 vs. the irradiation time of 1.3% Au-$BiOCl_{1-x}Br_x$ and $BiOCl_{1-x}Br_x$, respectively; (a) x = 1, (b) x = 0.75, (c) = 0.5, (d) = 0.25 and (e) = 0; (f) Photocatalytic degradation efficiency of phenol under simulated solar light irradiation over the Au-$BiOCl_{0.25}Br_{0.75}$ composites.

1.3% Au-$BiOCl_{0.25}Br_{0.75}$ composite. The lattice fringe with the d-spacing of 0.347 corresponds to the (101) crystallographic plane of $BiOCl_{0.25}Br_{0.75}$, whereas the presence of (111) crystallographic plane of Au has a lattice space of 0.347 nm. Moreover, the continuity of the lattice fringes and a distinguished interface in the 1.3% Au-$BiOCl_{0.25}Br_{0.75}$ composite can be observed, indicating that the intact heterojunction was successfully formed between Au NPs and $BiOCl_{0.25}Br_{0.75}$ composite.

The photocatalytic performance of as-synthesized $BiOCl_{1-x}Br_x$ (x = 0, 0.25, 0.5, 0.75 and 1) solid solutions and 1.3% Au-$BiOCl_{1-x}Br_x$ heterojunctions were first examined in terms of phenol solution photodegradation under simulated solar light irradiation. The concentration changement of phenol aqueous solution versus degradation time was shown in Fig. 3(a)–(e), and all the Au-$BiOCl_{1-x}Br_x$ heterojunctions display enhancement in the phenol solution degradation process. Moreover, it is clearly observed that the 1.3% Au-$BiOCl_{0.25}Br_{0.75}$ exhibited the best photoactivity. It can be observed that the degradation of phenol over pure $BiOCl_{0.25}Br_{0.75}$ is 31.4% after 75 min of simulated solar light irradiation. Compared to this, with the deposition of Au, the photocatalytic degradation efficiency of phenol over 1.3% Au-$BiOCl_{0.25}Br_{0.75}$ can increase at 98.5% under the same irradiation time, which also means that Au NPs have a significant influence. The photodegradation of the phenol as a function of the irradiation time over 1.3% Au-$BiOCl_{0.25}Br_{0.75}$ composite was presented in Fig. 3f. It can be clearly seen that the absorption intensity decreases gradually as time increasing, and the maximum absorption wavelength of phenol at about 269 nm. As shown in Fig. 3f, the phenol photodegradation efficiency is nearly 100% when the simulated solar light was irradiated for 75 min which indicates that the 1.3% Au-$BiOCl_{0.25}Br_{0.75}$ composites possess superior activity for phenol degradation.

The detailed analysis of photocatalytic degradation of phenol solution on different photocatalysts was fitted into pseudo-first-order kinetics [26]

$$\ln(C/C_0) = kt \quad (1)$$

where C, C_0, k and t are the concentration of the phenol solution at t = 0 and t, the apparent reaction rate constant and the degradation time, respectively. As shown in Fig. 4, the calculated k values for phenol degradation through 1.3% Au-BiOBr, 1.3% Au-$BiOCl_{0.25}Br_{0.75}$, 1.3% Au-$BiOCl_{0.5}Br_{0.5}$, 1.3% Au-$BiOCl_{0.75}Br_{0.25}$ and 1.3% Au-BiOCl are 0.0242, 0.0365, 0.0196, 0.0220 and 0.0084 min^{-1}, respectively. The constant of 1.3% Au-$BiOCl_{0.25}Br_{0.75}$ (0.0365 min^{-1}) is found to be about 1.5 times that of 1.3% Au-BiOBr (0.0242 min^{-1}) and 4.3 times that of 1.3% Au-BiOCl (0.0084 min^{-1}), which also could illustrate the optimum ratio of Cl and Br achieves in this composite.

The photocatalytic performance of Au-$BiOCl_{0.25}Br_{0.75}$ with different loading amounts of Au NPs under solar light was evaluated by tracking the degradation of phenol. The percentage of remaining phenol (C/C_0) was plotted versus the irradiation time shown in Fig. 5. All the Au-$BiOCl_{0.25}Br_{0.75}$ samples displayed enhancement in phenol degradation process. After 75min of simulated solar light irradiation, the degradation rates of phenol were 84.5%, 98.5% and 78.9% for Au/$BiOCl_{0.25}Br_{0.75}$ wt ratios of 0.65, 1.3 and 1.95%, respectively. It is observed that the 1.3% Au-$BiOCl_{0.25}Br_{0.75}$ exhibited the best photoactivity. The result shows the amount of Au NPs is a significant effect on the photocatalytic activity of Au-$BiOCl_{0.25}Br_{0.75}$ composite, and the Au-$BiOCl_{0.25}Br_{0.75}$ composite with optimal Au/$BiOCl_{0.25}Br_{0.75}$ wt ratio is 1.3%.

The optical absorption properties of samples were examined by the UV–vis DRS in the wavelength vary from 200 nm to 800 nm. Fig. 6a displays the UV–vis diffuse reflectance spectra of $BiOCl_{1-x}Br_x$ (x = 0, 0.25, 0.5, 0.75 and 1) solid solutions. The maximum absorption edges of the BiOCl, $BiOCl_{0.75}Br_{0.25}$, $BiOCl_{0.5}Br_{0.5}$, $BiOCl_{0.25}Br_{0.75}$ and BiOBr are approximately 368, 398, 418, 428 and 440 nm, respectively. Notablely, the $BiOCl_{1-x}Br_x$ solid solutions show an obvious red-shift of the absorption edges as x increases. While the absorption edges of 1.3% Au-$BiOCl_{1-x}Br_x$ composites are similar to that of $BiOCl_{1-x}Br_x$ apart from the absorption edges in visible light region, as shown in Fig. 6b. The 1.3% Au-$BiOCl_{1-x}Br_x$ samples have additional broad absorption peaks around 450–700 nm (Fig. 6b), which belongs to the typical peaks of the colloidal gold nanoparticles surface plasmon resonance (SPR), further demonstrating the formation of Au NPs on the surface of $BiOCl_{1-x}Br_x$ samples. With the decoration of Au NPs, the photoresponse of $BiOCl_{1-x}Br_x$ samples have been successfully extended to the visible-light region. Therefore, the as-prepared Au-$BiOCl_{1-x}Br_x$ composites have broad absorption in the visible range and enhancing the light absorption. It suggests that the Au-$BiOCl_{1-x}Br_x$ composites can be excited to generate more photo-induced electron-hole pairs, so as to increase the photocatalytic activity (Fig. 3). The UV–vis diffuse reflectance spectra of Au nanoparticles (Au NPs) before and after modifying with $BiOCl_{0.25}Br_{0.75}$ have been shown in Fig. 6c. Pure Au NPs displayed absorption peak centered at about 532 nm, which was ascribed to SPR absorption of Au NPs. In

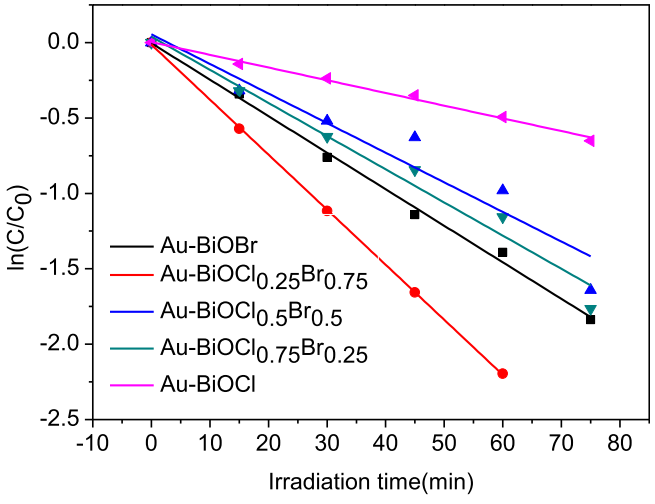

Fig. 4. Plot of ln (C/C_0) against the irradiation time under simulated solar light irradiation over the Au-$BiOCl_{1-x}Br_x$ composites.

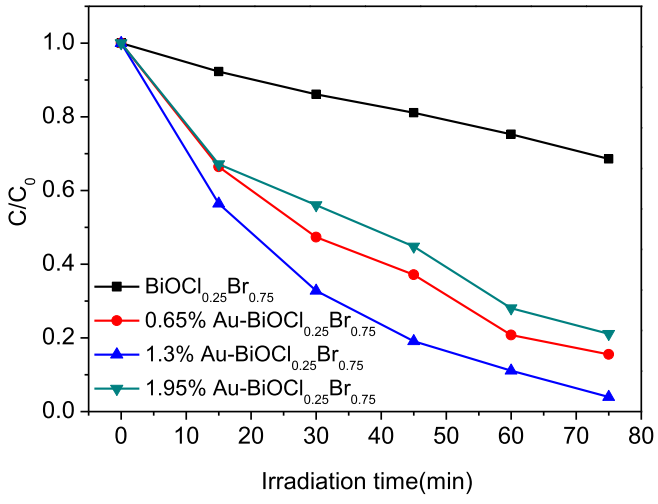

Fig. 5. Plots of C/C_0 vs. the irradiation time for the degradation of phenol over different weight ratios of Au/$BiOCl_{0.25}Br_{0.75}$ samples under solar light irradiation.

contrast, $BiOCl_{0.25}Br_{0.75}$ alone shows no obvious absorption in visible wavelength range. Additionally, a red shift of SPR absorption peak from 532 to 549 nm has been observed, demonstrating that Au NPs have been deposited onto the $BiOCl_{0.25}Br_{0.75}$. For the Au-$BiOCl_{0.25}Br_{0.75}$ composites, the SPR peaks were weaker and broader than that of pure Au. The SPR absorption peak position depends on particle size and the amount of Au particles. The comparison of UV–vis spectra of Au-$BiOCl_{0.25}Br_{0.75}$ composites with different loading amounts of Au NPs shows a trend that more Au NPs modifying induces bigger red shift. Based on the DRS results, the band gap energy of composites can be calculated by the formula

$$A(h\nu - Eg)^{n/2} = \alpha h\nu \quad (2)$$

where *Eg*, A, *a*, *v* and *h* are the band gap energy, constant, absorption coefficient, light frequency and Plank constant, respectively. In this formula, n is decided by the features of optical transition (n = 1 is for straight transition, n = 4 is for indirect optical transition). The plot of $(ahv)^{1/2}$ versus hv is depicted in Fig. 6d. According to this equation, the *Eg* values of $BiOCl_{1-x}Br_x$ solid solutions are ranging from 2.81 eV to 3.35eV as x increases from 0 to 1. The result indicates that $BiOCl_{1-x}Br_x$ solid solutions have adjustable band gap energy by control the mole ratio of Cl and Br. The valence band (VB) and conduction band (CB) of a photocatalyst are significant factors for the effective photocatalytic degradation of organic contaminants. The VB and CB of a semiconductor can be predicted by the equation [27–29]

$$E_{CB} = X - E_C - 0.5E_g \quad (3)$$

$$E_{VB} = E_{CB} + E_g \quad (4)$$

where X is the absolute electronegativity of all the constituent atoms, Ec and Eg are the energy of free electrons on the hydrogen scale (4.5 eV) and the band gap of the semiconductor. According to above empirical expressions, the E_{VB} and E_{CB} of the $BiOCl_{1-x}Br_x$ solid solutions were calculated and the results are listed in Table 1. As can be seen, the VB potentials of as-prepared $BiOCl_{1-x}Br_x$ solid solutions are 3.54, 3.35, 3.26, 3.16 and 3.09 eV when x is ranging from 0 to 1, which of those are more positive than the redox potentials of $\cdot OH/OH^-$ (1.99 eV), suggesting that the composites might have strong oxidation abilities. While the conduction band (CB) of $BiOCl_{1-x}Br_x$ (x = 0, 0.25, 0.5, 0.75 and 1) would appear at approximately 0.19, 0.30, 0.29, 0.28 and 0.28 eV, respectively.

In the photocatalytic degradation reaction (in Fig. 3), the activity is affected by the recombination rate of the photogenerated electrons and holes. The photoelectrochemical measurements were

Fig. 6. UV–vis DRS spectrum of the as-prepared (a) $BiOCl_{1-x}Br_x$; (b) 1.3% Au-$BiOCl_{1-x}Br_x$; (c) pure $BiOCl_{0.25}Br_{0.75}$, pure Au NPs and Au/$BiOCl_{0.25}Br_{0.75}$ samples; (d) Plot of the $(\alpha h\nu)^{1/2}$ versus hν of $BiOCl_{1-x}Br_x$ samples (x = 0, 0.25, 0.5, 0.75, 1).

Table 1
Absolute electronegativity, band gap energy, the VB edge and CB edge of as-synthesized $BiOCl_{1-x}Br_x$ (x = 0, 0.25, 0.5, 0.75 and 1).

	X (eV)	E_g (eV)	E_{VB} (eV)	E_{CB} (eV)
BiOCl	6.36	3.35	3.54	0.19
$BiOCl_{0.75}Br_{0.25}$	6.32	3.05	3.35	0.30
$BiOCl_{0.5}Br_{0.5}$	6.27	2.97	3.26	0.29
$BiOCl_{0.25}Br_{0.75}$	6.22	2.88	3.16	0.28
BiOBr	6.18	2.81	3.09	0.28

carried out by researching the photocurrent of as-prepared samples under the solar light irradiation, as shown in Fig. 7. It is clearly that a periodic response to light-on and light-off at an interval of 10s, which indicating the composites are prompt in generating photocurrent due to the effective separation of the photoinduced carriers. 1.3% Au-$BiOCl_{1-x}Br_x$ (x = 0, 0.25, 0.5, 0.75 and 1) composites modified ITO electrode show higher photocurrent than the $BiOCl_{1-x}Br_x$ solid solutions modified ITO electrode. The higher photocurrent intensity indicates that the recombination rate of photogenerated electrons and holes is lower in the photocatalytic procedure. The apparent enhanced photocurrent indicates the strong photoelectrochemical response of $BiOCl_{1-x}Br_x$ by the addition of Au NPs. The result further demonstrates photogenerated electron-hole pairs of the Au-$BiOCl_{1-x}Br_x$ composites have less recombination probability and more efficient separation efficiency, thus leading to superior photodegradation efficiency of phenol under the simulated solar light irradiation. The possible reasons are summarized as follows: The SPR of Au NPs could be excited under visible light region, which increases the probability of the photoexcitation of interfacial electrons. Therefore, Au NPs are beneficial to capture and transfer the optical excitation electrons, promoting the separation efficiency of electrons and holes pairs.

In order to ascertain the photocatalytic mechanism of Au-$BiOCl_{1-x}Br_x$ composites, it is important to detect the major active species for the photodegradation of phenol under simulated solar light irradiation. Therefore, several sacrificial agents were applied to quench the active species in the reaction system. Herein, ammonium oxalate (AO) was employed to scavenge holes (h^+), benzoquinone (BQ) for superoxide radicals ($\cdot O_2^-$) and isopropyl alcohol (IPA) for hydroxyl radicals (•OH), respectively. As shown in Fig. 8, the photocatalytic degradation of phenol solution over Au-$BiOCl_{0.25}Br_{0.75}$ is affected slightly by adding BQ, indicating the $\cdot O_2^-$ active species have a little influence during the solar light photodegradation process. However, the photocatalytic activities are strongly inhibited in the presence of AO and IPA. As a consequence, hydroxyl radicals (•OH) and holes (h^+) should be main active species of Au-$BiOCl_{0.25}Br_{0.75}$ in phenol solution and play important roles in phenol photodegradation process.

A possible mechanism for phenol degradation by the Au-$BiOCl_{1-x}Br_x$ composites has been illustrated in Fig. 9. Typically, upon the irradiation of Au-$BiOCl_{1-x}Br_x$ composites with solar light, the electrons of composite are excited from the VB of $BiOCl_{1-x}Br_x$ to the CB of $BiOCl_{1-x}Br_x$. The electrons in the conduction band further transfer to the Au nanoparticles (Au NPs) in the Au-$BiOCl_{1-x}Br_x$ composites because of the high work function of Au [30], which is beneficial for the efficient separation of photo-generated electron-hole pairs. As for the Au NPs, simulated solar light irradiation (450–700 nm) induces SPR and produces electrons, leaving holes in Au NPs. The Au nanoparticles work as an electron buffer [31] to accept photo-generated electrons from the CB of $BiOCl_{1-x}Br_x$, effectively preventing recombination of the electron-hole pairs. And the excited electrons to scavenge oxygen molecules in aqueous solution to form superoxide radicals and simultaneously the $\cdot O_2^-$ would further oxidize H_2O into •OH. Meanwhile, the holes remain at the VB of $BiOCl_{1-x}Br_x$ and on the surface of Au NPs can oxidize the phenol by reacting with the water to generate hydroxyl radical (•OH). Both •OH radicals and $\cdot O_2^-$ radicals are highly reactive for photodegradation of phenol. Furthermore, the transfer of electrons from $BiOCl_{1-x}Br_x$ to the Au NPs supports better spatial charge separation and prevents direct recombination of electron-hole

Fig. 7. Photocurrent responses of $BiOCl_{1-x}Br_x$ and 1.3%Au-$BiOCl_{1-x}Br_x$.

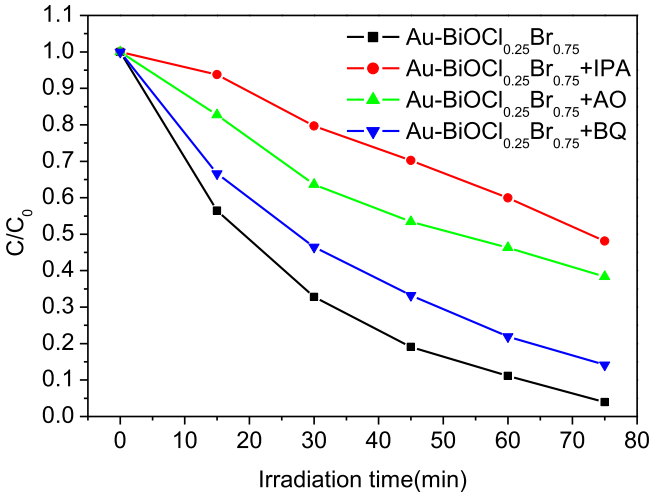

Fig. 8. Effects of radical scavengers in the photodegradation process of phenol over 1.3%Au-$BiOCl_{0.25}Br_{0.75}$.

pairs, thus improving the quantum efficiency. As we know, the electrons would recombine with the holes in Au NPs to a certain degree. However, the effect of gold nanoparticles is to promote the separation of electron-hole pairs of $BiOCl_{1-x}Br_x$ solid solutions, so as to improve the photocatalytic performance. And the effect of the recombination rate of the electron-hole pairs on the Au nanoparticles is secondary in the photocatalytic process. Hence, the enhanced photocatalytic activity observed for Au-$BiOCl_{1-x}Br_x$ composites in comparison with $BiOCl_{1-x}Br_x$, is likely contributed by following reasons: Firstly, the surface plasmon resonance (SPR) of Au NPs plays an important role in the light absorption capacity and extends the utilization of visible light, which can be confirmed by the UV–vis diffuse reflectance spectra (Fig. 6c). Then, with loading of Au NPs, the SPR not only facilitates the surface electron excitation but also the interfacial electron transfer, which improves the effective separation of electrons and holes under solar light irradiation (Fig. 7). On the other hand, the VB potentials of $BiOCl_{1-x}Br_x$ become more negative as the increasing content of Br (Table 1), which suggesting the redox abilities of holes on the VB of solid solutions grow weaker, whereas the light absorption becomes stronger (Fig. 6a). Finally, the energy band positions are tunable by changing the mole ratio of Cl and Br, which indicates that the Au-$BiOCl_{0.25}Br_{0.75}$ has a bandgap suitable, and achieves the desired enhancement in the photocatalytic degration of phenol under the solar light irradiation.

Fig. 9. Schematic diagram of the photocatalysis process over Au-$BiOCl_{0.25}Br_{0.75}$ composite.

4. Conclusion

In summary, the Au-$BiOCl_{1-x}Br_x$ composites were synthesized via a simple process using precipitation and assisted sonication methods. The resulting 1.3% Au-$BiOCl_{0.25}Br_{0.75}$ composite exhibits the excellent photocatalytic activity of phenol degradation under simulated solar light irradiation. The SPR effect of Au NPs plays an important role in the enhancement of photocatalytic performance, which would be beneficial to the light absorption capacity and the photo-generated charge separation. In the photocatalytic mechanism, hydroxyl radicals (•OH) and holes (h^+) were found to be the main active species, and $\bullet O_2^-$ showed a minor contribution by using active species scavengers. Moreover, this composite could be easily prepared and further applied in relative practical applications.

Acknowledgment

This work is financially supported by the National Nature Science Foundation of China (No. 21273034).

References

[1] Z. Wei, F.F. Liang, Y.F. Liu, W.J. Luo, J. Wang, W.Q. Yao, Y.F. Zhu, Appl. Catal. B-Environ 201 (2017) 600–606.
[2] M.C. Long, W.M. Cai, J. Cai, B.X. Zhou, X.Y. Chai, Y.H. Wu, J. Phys. Chem. B 110 (2006) 20211–20216.
[3] D.Z. Lu, M.C. Yang, P.F. Fang, C.H. Li, L.L. Jiang, Appl. Surf. Sci. 399 (2017) 167–184.
[4] H.F. Cheng, B.B. Huang, Y. Dai, Nanoscale 6 (2014) 2009–2026.
[5] L. Ye, J. Liu, C. Gong, L. Tian, T. Peng, L. Zan, ACS Catal. 2 (2012) 1677–1683.
[6] D. Zhang, J. Li, Q.G. Wang, Q.S. Wu, J. Mater. Chem. A 1 (2013) 8622–8629.
[7] K. Zhang, D. Zhang, J. Liu, K. Ren, H. Luo, Y. Peng, G. Li, X. Yu, Cryst. Eng. 14 (2012) 700–707.
[8] Y. Xu, X. Hu, H. Zhu, J. Zhang, J. Mater. Sci. 51 (2016) 4342–4348.
[9] J. Song, Q. Fan, W. Zhu, R. Wang, Z. Dong, Mater. Lett. 165 (2016) 14–18.
[10] Y.L. Qi, Y.F. Zheng, X.C. Song, J. Taiwan Inst. Chem. E 71 (2017) 355–363.
[11] J. Yuan, J. Wang, Y. She, J. Hu, P. Tao, F. Lv, Z. Lu, Y. Gu, J. Power Sources 263 (2014) 37–45.
[12] M.L. Chen, S. Yu, X.J. Zhang, F. Wang, Y.H. Lin, Y. Zhou, Superlattices Microstruct. 89 (2016) 275–281.
[13] Y. Feng, C.B. Liu, H.N. Che, J.B. Chen, K. Huang, C.Y. Huang, W.D. Shi, Cryst. Eng. Comm. 18 (2016) 1790–1799.
[14] H. Gnayem, Y. Sasson, ACS Catal. 3 (2013) 186–191.
[15] W.J. Kim, D. Pradhan, B.K. Min, Appl. Catal. B-Environ 147 (2014) 711–725.
[16] Z.F. Jia, F.M. Wang, F. Xin, B.Q. Zhang, Ind. Eng. Chem. Res. 50 (2011) 6688–6694.
[17] X.W. Wang, W.Y. Wang, Y.Q. Miao, G. Feng, R.B. Zhang, J. Colloid Interface Sci. 475 (2016) 112–118.
[18] H. Liu, Y. Su, Z. Chen, Z.T. Jin, Y. Wang, Sep. Purif. Technol. 133 (2014) 343–350.
[19] H.X. Lin, L.Y. Ding, Z.X. Pei, Y.G. Zhou, J.L. Long, W.H. Deng, X.X. Wang, Appl. Catal. B-Environ 160–161 (2014) 98–105.
[20] X.Q. Yan, X.H. Zhu, R.H. Li, W.X. Chen, J. Hazard. Mater (2016) 1–9.
[21] P.C. Yan, L. Xu, J.X. Xia, Y. Huang, J.X. Qiu, Q. Xu, Q. Zhang, H.M. Li, Talanta 156–157 (2016) 257–264.
[22] I. Majeed, M.A. Nadeem, E. Hussain, A. Badshah, R. Gilani, M.A. Nadeem, Int. J. Hydrogen Energy 42 (2017) 3006–3018.
[23] S. Yurdakal, B.S. Tek, C. Degirmenci, G. Palmisano, Catal. Today 281 (2017) 53–59.
[24] P. She, K.L. Xu, Q.R. He, S. Zeng, H. Sun, Z.N. Liu, J. Mater. Sci. 52 (2017) 3478–3489.
[25] T.Y. Liu, W. Chen, Y.X. Hua, X.H. Liu, Appl. Surf. Sci. 392 (2017) 616–623.
[26] Q.W. Cao, Y.F. Zheng, X.C. Song, Ceram. Int. 42 (2016) 14533–14542.
[27] X. Cui, Y.F. Zheng, H. Zhou, H.Y. Yin, X.C. Song, J. Taiwan Inst. Chem. E 60 (2016) 328–334.
[28] X. Cui, W.Z. Huang, H. Zhou, H.Y. Yin, Y.F. Zheng, X.C. Song, Curr. Nanosci. 11 (2015) 360–365.
[29] Q.W. Cao, Y.F. Zheng, H.Y. Yin, X.C. Song, J. Mater. Sci. 51 (2016) 4559–4565.
[30] H.Y. Jiang, K. Cheng, J. Lin, Phys. Chem. Chem. Phys. 14 (2012) 12114–12121.
[31] Q. Xiang, G.F. Meng, H.B. Zhao, Y. Zhang, H. Li, W.J. Ma, J.Q. Xu, J. Phys. Chem. C 114 (2010) 2049–2055.